

Thrust of Stovepipe Ramjet in Varying Mach Regimes

Pablo Arroyo, Wenyuan Hou, Razvan Pretorian, Anushka Tahiliani and Kazuki Tojo
Massachusetts Institute of Technology, Cambridge, MA, 02139

The paradox of thrust generation in a stovepipe ramjet is one that has been sparsely examined in the literature. Prior work has studied two simple cases of subsonic and supersonic heating, concluding that subsonic heating generates thrust via lip suction whilst supersonic heating results in zero thrust. This report investigates the accuracy and comprehensiveness of these results, through analytical and numerical control volume calculations, and finds that the prior work is correct but incomprehensive. The stovepipe ramjet problem is extended to two more cases, or "quadrants", of subsonic cooling and supersonic cooling, and identifies five regimes of possible flow solutions within the four total quadrants. A comprehensive analytical description of "Four Quadrants, Five Regimes" is provided, along with numerical validation for all but one regime. Preliminary numerical results are presented for the missing regime, serving as a stepping stool for future work to complete the full picture.

Nomenclature

p	=	Static pressure [Pa]
p_t	=	Stagnation (total) pressure [Pa]
ρ	=	Fluid density [kg/m^3]
T	=	Static temperature [K]
T_t	=	Stagnation temperature [K]
h_t	=	Stagnation enthalpy [J/kg]
u	=	Flow velocity [m/s]
M	=	Mach number, $M = u/a$ [-]
c_p	=	Specific heat at constant pressure [J/kg·K]
q	=	Heat added per unit mass [J/kg]
w_{shaft}	=	Shaft work per unit mass [J/kg]
R	=	Specific gas constant [J/kg·K]

$$a \quad = \quad \text{Speed of sound [m/s]}$$

I. Introduction

This project investigates the flow features and mechanisms responsible for thrust generation in thermally driven ducts, with particular attention to subsonic and supersonic regimes. The starting point for this work is a phenomenon identified by Oswatitsch [1], observed for a stovepipe ramjet: heat addition can produce net thrust in subsonic flow, but generates no thrust in the supersonic case. To analyze this behavior, we consider an idealized model consisting of a cylindrical tube with constant area placed in a uniform subsonic freestream with internal heat addition, as depicted in Fig. 1. The walls and heating source are assumed to be infinitesimally thin, with the heat input localized upstream of the tube exit. Under these assumptions, the jet exits at ambient pressure, and all pressure forces on the duct surfaces act normal to the flow.

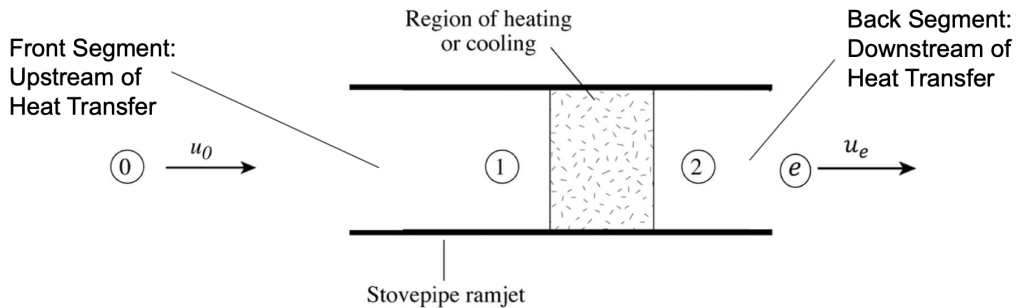


Fig. 1 Schematic of heated tube in uniform flow.

As shown in Fig. 1, the overall system can be divided into three regions:

- Region 0 → 1: upstream of heat addition,
- Region 1 → 2: the heat addition zone,
- Region 2 → e: downstream of heat addition.

The behavior of the flow can be characterized using quasi-one-dimensional compressible flow relationships, which reveal key trends across the heating region. In subsonic compressible flow, much like in the incompressible case, heat addition induces a pressure rise upstream and a pressure drop downstream. This pressure difference creates an accelerated region in the downstream segment. From a control volume perspective, a net thrust emerges despite the absence of axial pressure forces acting on the duct surfaces. Instead, the thrust arises from a suction effect at the upstream edge of the duct, resulting from the curvature of streamlines near the inlet.

While the subsonic solution offers basic insight, the behavior changes significantly past unity in the stovepipe ramjet. In the supersonic case, the upstream conditions remain unaffected as long as the flow remains supersonic through the heated region. Downstream, heat addition increases pressure and temperature, but the resulting expansion bell and

shock structures from supersonic overpressure lead to velocity deficits in the wake. Despite a local increase in velocity, the net thrust is zero due to shock losses and flow separation. The flow behavior described by Oswatitsch [1] can be represented in Figs. 2 and 3 for the subsonic and supersonic cases, respectively.

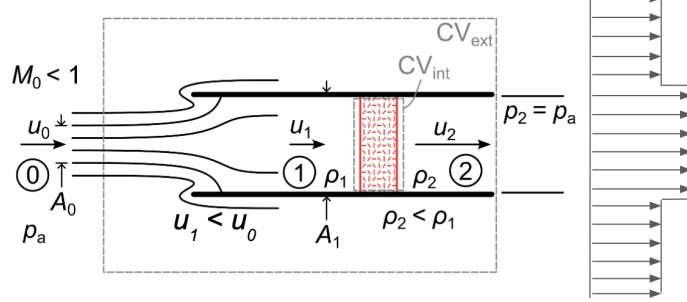


Fig. 2 Idealized subsonic ramjet configuration illustrating thrust generation in subsonic flow via heat addition, adapted from Oswatitsch [1].

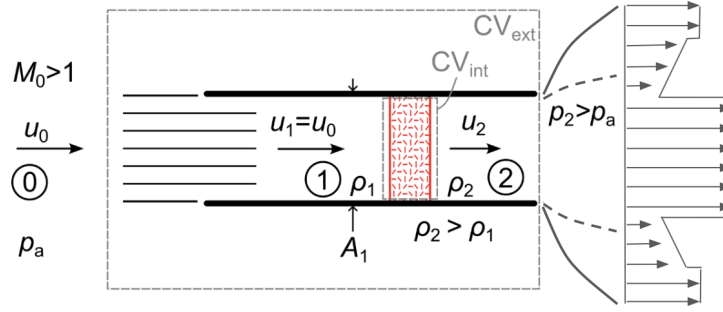


Fig. 3 Idealized supersonic ramjet configuration illustrating no thrust generation in supersonic flow via heat addition, adapted from Oswatitsch [1].

These contrasting behaviors highlight fundamental differences in how heat affects momentum in compressible flows. This work examines these effects using both analytical models and numerical computations, with the goal of clarifying the physical mechanisms and conditions under which thermal propulsion is possible. The apparent paradox motivates a deeper examination of how forces are transmitted in compressible flows with localized thermal input, whether through heating or cooling.

II. Background

To qualitatively assess the thrust-generation mechanism, the governing thermodynamic relationships are evaluated for each region. The analysis begins with the heat addition zone:

A. Heat Addition in a Duct

In a steady, one-dimensional flow through a constant-area duct, the first law of thermodynamics applied to a control volume yields the energy balance

$$h_{t2} - h_{t1} = q - w_{\text{shaft}}, \quad (1)$$

where h_t is the stagnation enthalpy, q is the heat added per unit mass, and w_{shaft} is the shaft work per unit mass. In the case of a stovepipe ramjet, there is no mechanical work done ($w_{\text{shaft}} = 0$), so all heat added directly contributes to an increase in stagnation enthalpy. Since stagnation enthalpy is directly related to stagnation temperature, T_t , for a perfect gas with constant specific heats, Eq. (1) can be simplified to

$$\Delta h_t = c_p \Delta T_t = q, \quad (2)$$

which indicates that heat addition in such a system leads to a direct increase in T_t .

As outlined by Shapiro [2], for compressible, frictionless (inviscid), constant-area flow with heat addition, the differential relationships between flow properties and stagnation temperature are

$$\frac{dM^2}{M^2} = \frac{(1 + \gamma M^2) \left(1 + \frac{\gamma-1}{2} M^2\right)}{1 - M^2} \cdot \frac{dT_t}{T_t}, \quad (3)$$

$$\frac{dp}{p} = -\frac{\gamma M^2 \left(1 + \frac{\gamma-1}{2} M^2\right)}{1 - M^2} \cdot \frac{dT_t}{T_t}, \quad (4)$$

$$\frac{dT}{T} = \frac{(1 - \gamma M^2) \left(1 + \frac{\gamma-1}{2} M^2\right)}{1 - M^2} \cdot \frac{dT_t}{T_t}, \quad (5)$$

$$\frac{d\rho}{\rho} = -\frac{1 + \frac{\gamma-1}{2} M^2}{1 - M^2} \cdot \frac{dT_t}{T_t}, \quad (6)$$

where γ is the ratio of specific heats, M is the local Mach number, p is static pressure, T is static temperature, and ρ is density.

These equations form the foundation for analyzing flow behavior in the region of heat addition and help predict the direction of local changes in the cases evaluated by Oswatitsch and the additional cooling cases evaluated in this report. To build intuition of the flow phenomenon, the analysis begins with the incompressible (low Mach number) limit, where simplifying assumptions allow for analytical treatment. This baseline case serves to assess the governing relationships before extending to compressible regimes.

B. Subsonic, Incompressible Stovepipe Ramjet

The first case—subsonic, incompressible flow with $M^2 \ll 1$ —can be computed analytically under the following simplifying assumptions. First, at very low Mach numbers under heat addition, the pressure variations are small relative to the ambient pressure, allowing the approximation $p \approx \text{constant}$. This is also supported by Eq. (4), which quantifies the inverse relationship between $\frac{dp}{p}$ and $\frac{dT_t}{T_t}$ in subsonic flows, the pressure drop across the heated region approaches zero in the limit $M^2 \ll 1$. Under these conditions, the ideal gas law reduces to

$$\rho T = \text{constant}. \quad (7)$$

However, the assumption of uniform density only holds true outside the heated region. Within the heated zone, the density change can be governed by

$$\frac{\rho_1}{\rho_2} = \frac{T_2}{T_1}, \quad (8)$$

where the local temperature rise leads to a corresponding drop in density. This inverse relation is consistent with the ideal gas law and is supported by both Eq. (5) and Eq. (6), where the increase in temperature due to heat addition is balanced by a corresponding decrease in density. Lastly, the flow is assumed to be inviscid, and the exit pressure is taken to equal atmospheric pressure. For the upstream region $0 \rightarrow 1$, Bernoulli's equation can be applied to relate static pressure and velocity, under the assumption of constant density, $\rho_0 = \rho_1$,

$$p_0 - p_1 = \frac{1}{2} \rho_0 (u_1^2 - u_0^2). \quad (9)$$

Within the region of constant-area heat addition, the continuity equation (Eq. 10), the equation of state, and the momentum equation (Eq. 11) can be used to describe the flow under the assumptions that $p_2 = p_0$ and $\rho_0 = \rho_1$. The continuity and momentum equations can be written as:

$$\rho_0 u_1 = \rho_2 u_2 \text{ and} \quad (10)$$

$$p_1 - p_2 = \rho_2 u_2^2 - \rho_0 u_1^2. \quad (11)$$

By rearranging Eqs. (9) and (11) to isolate the terms involving $p_0 - p_1$ and then equating them, followed by division by ρ_0 , the downstream velocity u_2 can be expressed in terms of the upstream velocity u_1 as

$$u_2^2 = \frac{1}{2} \left(\frac{\rho_0}{\rho_1} \right) (u_1^2 + u_0^2). \quad (12)$$

The force acting on the control volume encompassing the entire stovepipe ramjet, using the principle of conservation

of momentum, can be written as

$$F = \dot{m}(u_2 - u_0). \quad (13)$$

Here, \dot{m} is the mass flow rate, which remains conserved throughout the control volume. At station 1, it can be expressed as $\dot{m}_1 = \rho_0 A_1 u_1$, where ρ_0 is the density at station 1, A_1 is the cross-sectional area of the ramjet at station 1, and u_1 is the flow velocity at station 1.

All pressure forces acting on the ramjet surface are normal to the flow direction, or conversely, no axial force is exerted by the solid structure on the flow. However, a control volume analysis indicates that a momentum change occurs across the region of heat addition. Therefore, the thrust can only originate from the flow around the inlet lip, as identified by Oswatitsch [1].

The streamline pattern at the inlet, or the source of thrust production, is a function of the velocity ratio between the inlet flow and the ambient (onset) flow, u_1/u_0 , particularly in the subsonic regime. To analyze this, the continuity relation can be rearranged $u_1 = (\rho_2/\rho_0)u_2$ and used to express u_1 in terms of u_2 and the density ratio:

$$\frac{u_1}{u_0} = \sqrt{\frac{1}{2(\rho_0/\rho_2) - 1}} \quad (14)$$

$$\frac{u_2}{u_0} = \sqrt{\frac{\rho_0/\rho_2}{2 - (\rho_2/\rho_0)}} \quad (15)$$

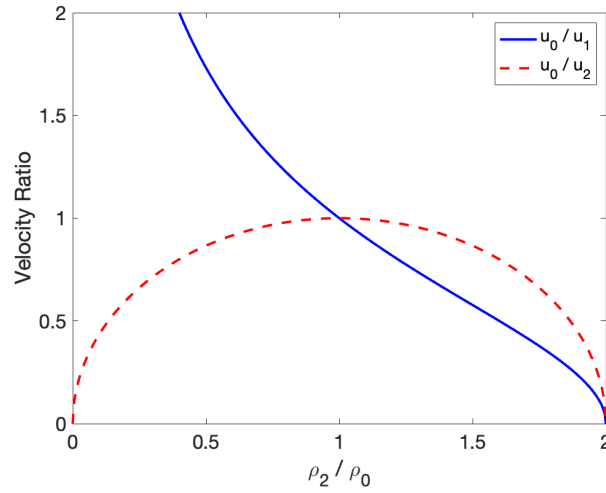


Fig. 4 u_1/u_0 and u_0/u_2 plotted as a function of the density ratio across the heat addition region, where $\rho_0 = \rho_1$.

The thrust expression in Eq. (13) can then be non-dimensionalized by the dynamic pressure $\frac{1}{2}\rho_0 u_0^2$ and duct area A ,

yielding

$$\tilde{F} \equiv \frac{F}{\frac{1}{2}\rho_0 A u_0^2} = 2 \left(\frac{u_1}{u_0} \right) \left(\frac{u_2}{u_0} - 1 \right). \quad (16)$$

From Eqs.(14) and (15), as well as Fig. 4, it is evident that when there is no heat addition, $\rho_0/\rho_2 = 1$, resulting in $u_1/u_0 = 1$ and $u_2/u_0 = 1$. Under this condition, the non-dimensional thrust becomes zero in Eq. (16). This unity in upstream velocity ratio ($u_1/u_0 = 1$) implies there is no pressure differential at the inlet lip to induce curvature in the streamlines—hence, no suction force and no generated thrust. In contrast, for any other condition involving heat addition or cooling (i.e., $\rho_0/\rho_2 \neq 1$), thrust is produced due to the net force created at the inlet.

C. Problem Statement

Having laid out Oswatitsch's previous work [1], we ask two questions. Was Oswatitsch correct and comprehensive? Furthermore, can the problem be quantified beyond Oswatitsch's qualitative descriptions?

To answer these questions, we conducted an analytical and numerical verification, as well as extension, of the work by Oswatitsch [1].

III. Report Structure

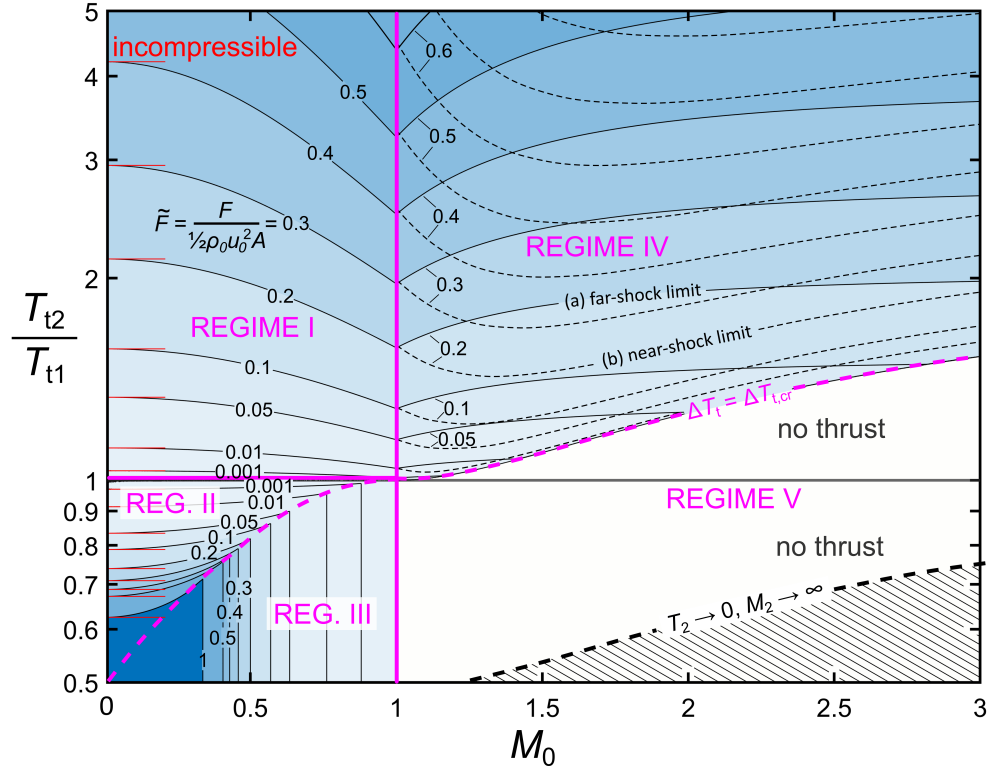


Fig. 5 Four quadrants of the stovepipe ramjet problem, showing analytically computed contours of normalized thrust as a function free stream Mach number and stagnation temperature ratio

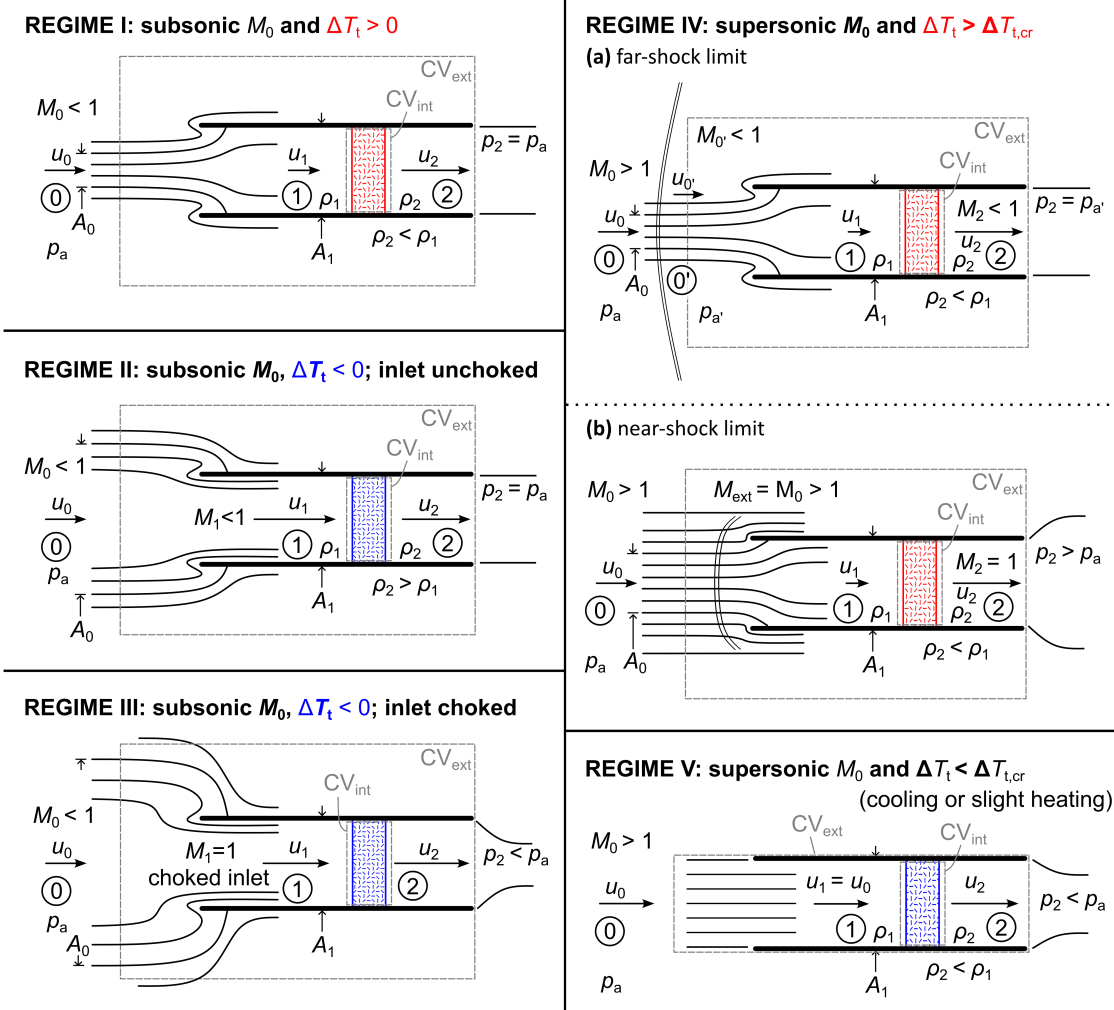


Fig. 6 Schematic of flow phenomenon for different regimes of freestream Mach number and heat addition.

There are four scenarios of the stovepipe ramjet problem: subsonic heating, subsonic cooling, supersonic heating and supersonic cooling. This report combines these scenarios into four quadrants (Fig. 5) of a plot of the heat addition/rejection, T_{t2}/T_{t1} , against the freestream Mach number, M_0 . In addition, amongst the four quadrants, we have identified five regimes of analytical solutions. These regimes are also labeled in Fig. 5, and their respective flowfields are portrayed in Fig. 6.

IV. Quadrant I: Subsonic Heating

A. Analytical Calculation

Subsonic heating is depicted in Regime I of Fig. 6. This section will apply quasi-one-dimensional compressible flow concepts to analyze this regime.

We start with the freestream Mach number, M_0 , and static conditions, T_0 and p_a , of the freestream. The stagnation

states are

$$T_{t0} = T_0 \left[1 + \frac{(\gamma - 1)M_0^2}{2} \right] \text{ and} \quad (17)$$

$$p_{t0} = p_a \left[1 + \frac{(\gamma - 1)M_0^2}{2} \right]^{\frac{\gamma}{\gamma-1}}. \quad (18)$$

Assuming adiabatic and reversible flow from station 0 to station 1, the stagnation states remain the same:

$$T_{t1} = T_{t0} \text{ and} \quad (19)$$

$$p_{t1} = p_{t0}. \quad (20)$$

M_1 is initially unknown and there does not exist a simple analytical expression for it in terms of the free stream conditions and heat addition ratio. Thus, a trial value of M_1 is selected in the range $[0, M_{1cr}]$, where M_{1cr} is the critical Mach number of the inlet flow that would choke in a frictionless constant-area duct after the stagnation temperature is raised by τ . The subsonic value of M_{1cr} is solved for in terms of τ using eq. 10.4.6 in [3] to obtain

$$M_{1cr}^2 = \frac{\tau(\gamma + 1) - \gamma - (\gamma + 1)\sqrt{\tau(\tau - 1)}}{\gamma^2 + \tau(1 - \gamma^2)}. \quad (21)$$

From M_1 , we calculate trial values of T_{t0} , p_{t0} . These trial values of M_1 , T_{t0} , and p_{t0} are in turn starting points for computing downstream conditions. The process is iterated until an M_1 is found such that the subsonic exit requirement is met, i.e., $p_2 = p_a$.

To calculate conditions at station 2, we start with the differential relationship between M^2 and T_t in a frictionless, constant-area duct (Eq.(3)). Rearranging Eq. (3) by separation of variables and partial fraction decomposition, we obtain

$$\left[\frac{1}{M^2} - \frac{2}{M^2 + 1/\gamma} + \frac{1}{M^2 + 2/(\gamma - 1)} \right] dM^2 = \frac{dT_t}{T_t}. \quad (22)$$

Eq. 22 is integrated from T_{t1} to T_{t2} to yield

$$\frac{M_2^4 + \frac{2}{\gamma-1}M_2^2}{M_2^4 + \frac{2}{\gamma}M_2^2 + \frac{1}{\gamma^2}} \beta_1 = \tau, \quad (23)$$

where

$$\beta_1 = \frac{(M_1^2 + 1/\gamma)^2}{M_1^2[M_1^2 + 2/(\gamma - 1)]} \text{ and } \tau = \frac{T_{t2}}{T_{t1}}.$$

Eq. 23 is solved for M_2^2 to obtain

$$M_2^2 = \begin{cases} \frac{\gamma - \frac{\tau}{\beta_1}(\gamma-1) - \sqrt{\frac{\tau}{\beta_1}(1-\gamma^2)+\gamma^2}}{\gamma(\frac{\tau}{\beta_1}-1)(\gamma-1)} & M_1 < 1 \\ \frac{\gamma - \frac{\tau}{\beta_1}(\gamma-1) + \sqrt{\frac{\tau}{\beta_1}(1-\gamma^2)+\gamma^2}}{\gamma(\frac{\tau}{\beta_1}-1)(\gamma-1)} & M_1 > 1. \end{cases} \quad (24)$$

Eq. 24 is equivalent to Eq. 7.14 and curves of M_2 versus M_1 for constant-area heat addition in Fig. 7.5 of [4], but recast as an explicit expression of M_2 .

T_2 and u_2 can be computed from M_2 :

$$T_2 = \tau T_{t1} \left[1 + \frac{(\gamma-1)M_2^2}{2} \right]^{-1} \quad \text{and} \quad (25)$$

$$u_2 = M_2 \sqrt{\gamma R T_2} \quad (26)$$

The trial value for p_2 can now be computed using the conservation of momentum across the heat addition zone (CV_{int} in Fig. 6):

$$\dot{m}(u_2 - u_1) = A(p_1 - p_2), \quad (27)$$

which, assuming a perfect gas, becomes

$$p_2 = p_1 \left[1 - \gamma M_1 (M_2 \sqrt{\tau} - M_1) \right]. \quad (28)$$

Eqs. 24-28 are solved iteratively in MATLAB to find the inlet condition (i.e., M_1) that would result in the exit condition $p_2 = p_a$ required for a subsonic jet. The procedure is restated in the summary below:

- 1) Compute inlet stagnation quantities T_{t0} and p_{t0}
- 2) Guess a trial value for M_1 between 0 and M_{cr}
- 3) Compute p_1 and T_1 from the M_1 trial value and stagnation conditions
- 4) Compute u_1 from M_1 and T_1
- 5) Compute M_2 starting from M_1 and integrating from T_{t1} and T_{t2}
- 6) Compute T_2 from T_{t2}/T_{t1} , T_{t0} , and M_2
- 7) Compute u_2 from T_2 and M_2
- 8) Compute p_2 using p_1 , u_1 , and u_2 and conservation of momentum over CV_{int}
- 9) Iterate over steps 2-8 until $p_2 = p_a$

Finally, the thrust F is computed using u_0 , u_1 , u_2 and conservation of mass and momentum over CV_{ext} (see Fig. 6).

The solution method for this step is the same as the procedure in CQ-18 of Module 3 (adapted from Problem 5.12 of [2]). The CV_{ext} is drawn far away from the inlet such that the static pressure is uniform over the control surface, leaving only the velocity terms in the formula for thrust, as seen in Eq. (13).

The compressible normalized thrust is now

$$\tilde{F} \equiv \frac{F}{\frac{1}{2}\rho_0 u_0^2 A_1} = 2 \frac{p_1}{p_0} \frac{T_0}{T_1} \frac{u_1}{u_0} \left(\frac{u_2}{u_1} - 1 \right). \quad (29)$$

Note that \tilde{F} is a function of only M_0 and τ because each of the ratios on the right hand side of Eq. 29 are in principle functions of M_0 and τ . Here it is expressed in terms of intermediate quantities because there is no clean, explicit expression as far as we are aware.

The normalized thrust is computed over a grid of cases in the range $0 < M_0 < 1$ and $1 < T_{t2}/T_{t1} < 5$ and the result is shown in regime I of Fig. 5. Fig. 5 is overlaid with contours of normalized thrust from the incompressible calculation in eq. 16. Comparing the two sets of contours reveals that subsonic compressible flows behave similar to the incompressible case. Compressible effects increase the thrust only marginally at low Mach numbers, but by around 1.5X as M_0 approaches unity.

B. Numerical Calculation

1. Computational Setup

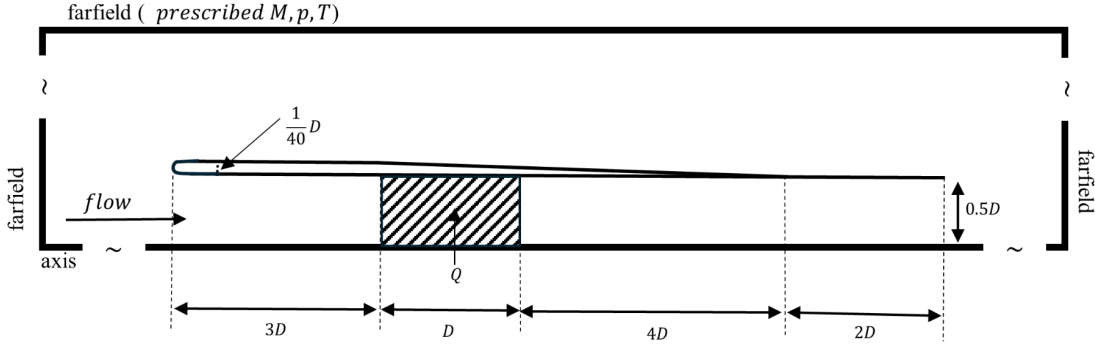


Fig. 7 Domain and duct geometry of subsonic CFD calculations.

To set up the stove pipe ramjet in ANSYS Fluent, a constant-area half-pipe was placed in a domain sufficiently large ($\sim 50D$) to allow the freestream flow to remain unaffected by the duct, as well as to let the exit flow resolve naturally before the end of the domain. To best capture inlet lip suction and a straight exit jet, the leading edge of the duct was curved via a conic section with a finite radius and a discretisation of ~ 100 cells along it was found to be satisfactory. The trailing edge was made to be a zero thickness flat surface. A schematic of the geometric setup is shown in Fig. 7.

The duct dimensions are scaled with the duct diameter D,

The cell count was approximately 100k within the entire domain. The problem is treated as 2D, axisymmetric, inviscid and compressible, using a second-order discretisation with a pseudo-transient method and relaxation.

2. Thrust

To compute normalised thrust, Section IV.A shows that it suffices to obtain the axial velocity and density at the freestream and the exit jet. Using the equation of state, Eq. 29 can be expressed as

$$\tilde{F} = 2 \frac{\rho_2}{\rho_0} \frac{u_2}{u_0} \left(\frac{u_2}{u_0} - 1 \right), \quad (30)$$

where u and ρ are axial velocity and density, respectively, at the freestream, position 0, and the jet exit, position 2.

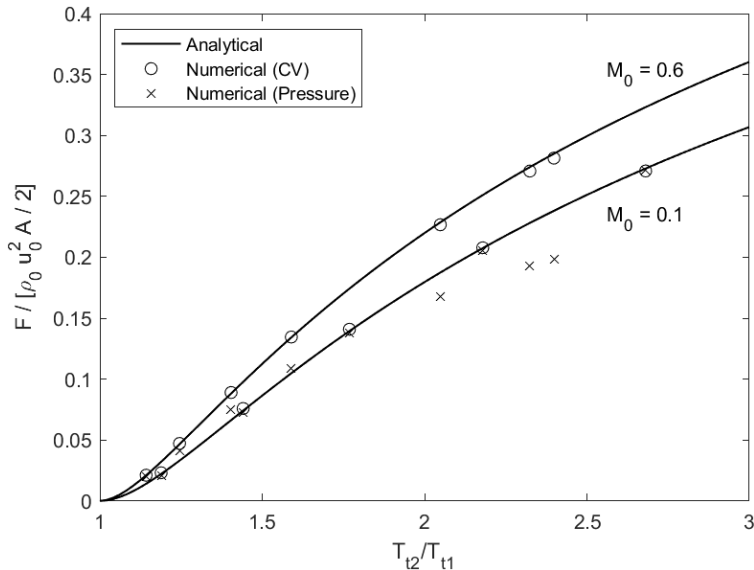


Fig. 8 Normalised thrust for subsonic heating at freestream Mach numbers of 0.1 and 0.6. Numerical results (circles) are consistent with the analytical curves.

Fig. 8 displays a comparison between the analytical solution for normalised thrust and data points from numerical calculations. To demonstrate the problem in both incompressible and compressible cases, CFD simulations were run at freestream Mach numbers of 0.1 and 0.6. The figure also includes normalised thrust calculated by integrating the pressure in the entire domain, which appears to be very accurate for $M_0 = 0.1$ but significantly underestimates for $M_0 = 0.6$. The inaccuracy of the pressure integral method was expected as it is more vulnerable to numerical errors. Overall, the numerical thrusts are very consistent with the analytical thrusts for Regime I, the subsonic heating case.

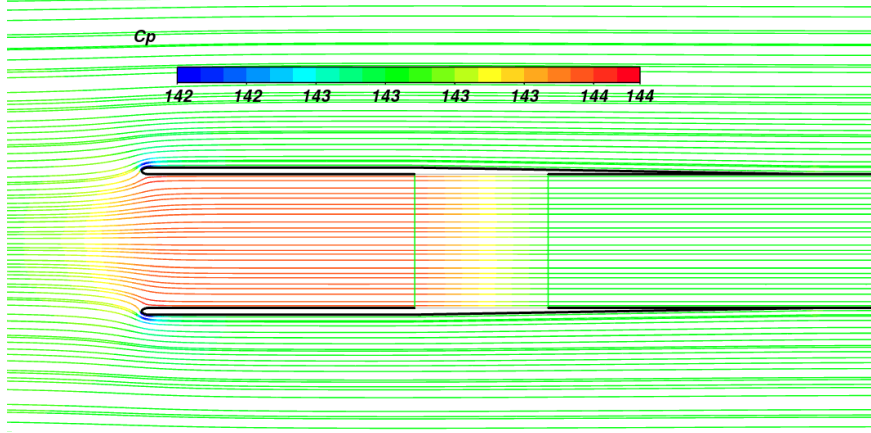


Fig. 9 Streamlines for subsonic heating at a freestream Mach number of 0.1. The streamline curvature is consistent with the analytical lip suction result.

3. Flow Topology

Similar to the thrust, the numerical streamlines (Fig. 9) were consistent with results from the analytical work. The streamline curvature, along with the lowered pressure at the lip, depict the lip suction generating thrust.

V. Quadrant II: Subsonic Cooling

A. Analytical Calculation

The subsonic cooling quadrant is subdivided into two regimes (see Fig. 5). In Regime II, the ratio of stagnation temperatures, T_{t2}/T_{t1} , is close to unity, and the flow behaves in a similar manner to the incompressible regime. In this regime, the flow is analyzed using the same procedure as the subsonic heating regime (see Sec. IV.A). The flow accelerates from station 0 to station 1 and decelerates during cooling from station 1 to station 2. Overall, the flow is accelerated from 0 to 2. Thus, our control volume analysis over CV_{ext} in Fig. 6 yields positive thrust, consistent with the inlet lip suction force.

In Regime III, the suction generated from the cooling is strong enough for the flow to choke at station 1. Further cooling in this regime cannot affect the flow upstream of station 1. Thus, thrust becomes a function of Mach number alone, as depicted by the vertical contours in Fig. 5. As the sonic flow from station 1 is cooled, it may take either the sub- or supersonic branches of the Rayleigh curve. Flow taking the subsonic branch becomes fundamentally two-dimensional when it adjusts to the pressure field upon approaching the exit, and this cannot be resolved within our quasi-1D framework. In contrast, flow taking the supersonic branch may exit as a supersonic jet. This is the scenario we analyze and show in Figs. 5 and IV.A. Because the jet exits at a finite pressure difference from ambient, the thrust equation must be modified to include the contribution from the pressure difference:

$$\tilde{F} = 2 \frac{p_1}{p_0} \frac{T_0}{T_1} \frac{u_1}{u_0} \left(\frac{u_2}{u_1} - 1 \right) + \frac{2}{\gamma M_0^2} \left(\frac{p_2}{p_0} - 1 \right). \quad (31)$$

Cooling along the supersonic branch of the Rayleigh curve both accelerate the flow and decrease the static pressure. These two effects perfectly cancel when determining thrust from the control volume approach, consistent with the observation that flow around the inlet (and thus the lip suction force) cannot adjust once station 1 is choked. Future work could involve a 2D description of the subsonic exit case and associated 2D conditions that govern whether the flow takes the sub- or supersonic branch of the Rayleigh curve.

B. Numerical Calculation

1. Computational Setup

The ANSYS Fluent setup for the subsonic cooling case was identical to that for subsonic heating (Fig. 7). Numerical calculations were performed to validate the analytical results of both Regime II and Regime III (Fig. 6), the two solutions for subsonic cooling.

2. Thrust

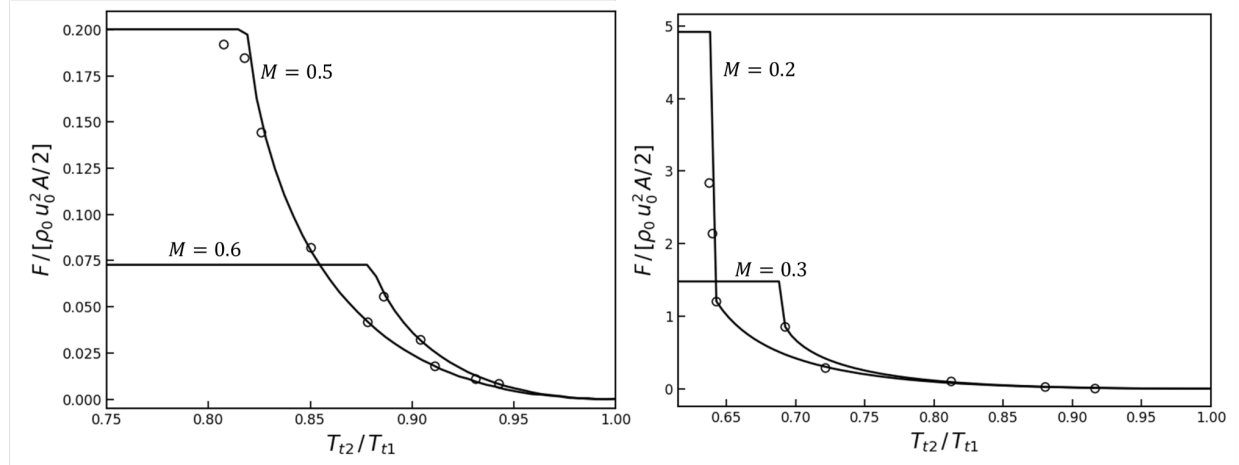


Fig. 10 Normalised thrust for subsonic cooling at freestream Mach numbers ranging from 0.2 to 0.6. Numerical results (circles) are consistent with the analytical curves.

The thrusts obtained from numerical calculations of subsonic cooling between $M_0 = 0.2$ and $M_0 = 0.6$ agree strongly with the analytical curve. It is particularly interesting to see the transitions from Regime II to Regime III, where the inlet chokes and thrust remains constant with further cooling.

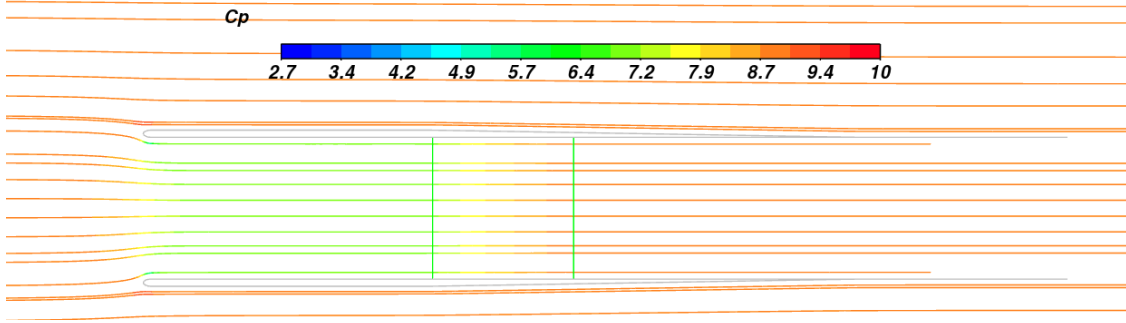


Fig. 11 Streamlines for subsonic cooling at a freestream Mach number of 0.4. The streamline curvature is consistent with the analytical lip suction result.

3. Flow Topology

Similarly, the streamlines from ANSYS Fluent are as expected based on analytical calculations. The streamline curvature and lip suction are well depicted.

VI. Quadrant III: Supersonic Heating

A. Analytical Calculation

1. Thrust

The supersonic heating quadrant consists of two regimes determined by whether the heat addition is enough to thermally choke the flow. Thermal choking occurs at the critical stagnation temperature ratio given by

$$\tau_{\text{cr}} = \frac{(1 + \gamma M_0^2)^2}{2(\gamma + 1)M_0^2 \left[1 + \left(\frac{\gamma - 1}{2} \right) M_0^2 \right]} \quad (32)$$

In Regime V, $T_{t2}/T_{t1} < \tau_{\text{cr}}$, and the flow remains supersonic throughout the duct. The flow is unchanged from station 0 to station 1. Flow properties at station 2 are calculated using Eqs. 24-28. A control volume analysis on CV_{ext} reveals that thrust is zero; the velocity term in the thrust equation (Eq. 31) exactly cancels with the pressure term. This is expected: without any change in the flow going from station 0 to station 1, CV_{int} , which was used to compute p_2 , sees the same entering and exiting flows as CV_{ext} . The zero-thrust result is also consistent with the flow topology, as neither the supersonic inlet or exit flow can produce thrust on an infinitesimally thin duct wall.

In Regime IV, $T_{t2}/T_{t1} > \tau_{\text{cr}}$, and the flow must adjust via a shock before entering the duct. Resolving the shock location and flow topology in this regime is inherently a 2D problem. However, we may assess two limiting cases using the quasi-1D framework. The two limits, denoted (a) far-shock limit and (b) near-shock limit, are depicted in Fig. 6.

In Regime IV(a), the far-shock limit, the stovepipe induces a broad normal shock sufficiently distant from the inlet

such that the entire flow field within and surrounding the duct is subsonic. This reduces to the subsonic heating case, but with free stream conditions replaced by $M_{0'}$, $T_{0'}$, and $p_{a'}$ calculated from normal shock relations.

In Regime IV(b), the near-shock limit, the shock stands near the inlet, just enough to allow the flow entering the duct to adjust to meet the thermal choking requirement at station 2. As a simplifying assumption, the external flow is completely unaffected by the inlet shock and remains at free stream conditions. Taking station 2 to be choked, the flow conditions at stations 1 and 0 can be computed. We start by computing M_1 using Eq. 24 in reverse (i.e. swapping the indices 1 and 2, and inverting τ). The stagnation states at station 1 are known ($T_{t1} = T_{t0}$, and p_{t1} may be calculated from p_{t0} using the normal shock relation). The remaining states are calculated using Eqs. 17-28 and the normalized thrust is calculated from CV_{ext} using Eq. 31.

Analytical thrust predictions for the two limiting cases are shown in Regime IV of Fig. 5: thrust contours from the far-shock limit are indicated by solid lines while those from the near-shock limit are indicated by broken lines. In either limit, the thrust force originates from lip suction as subsonic flow curves around the inlet post-shock. Future work could involve 2D analysis exploring real flows, which lie between these idealized limits as seen in Figs. 25-29.

2. Shocks

The pressure inside the stovepipe ramjet rises according to Eq. 4 from the freestream to the post-heating pressure. This higher pressure will cause streamlines to diverge once the flow exits the tube and forces the supersonic freestream around the ramjet to adjust. The equilibrium between the adjustment of the freestream and the expansion of the heated flow occurs when $p_{expansion} = p_{shock}$, where $p_{expansion}$ is the static pressure after the expansion of the heated flow and p_{shock} is the static pressure downstream of the oblique shock. The pressure ratio across an oblique shock is given by

$$\frac{p_{shock}}{p_0} = \frac{2\gamma M_0^2 \sin^2 \beta - (\gamma - 1)}{(\gamma + 1)}, \quad (33)$$

where γ is the specific heat ratio, M_0 is the Mach number, and β is the angle the oblique shock makes relative to the horizontal as defined by

$$\cot \theta = \tan \beta \left(\frac{(\gamma + 1) M_0^2}{2(M_0^2 \sin^2 s - 1)} - 1 \right), \quad (34)$$

where θ is the angle of the line where the post-shock flow and heated flow initially meet, measured from the horizontal. This angle will determine the conditions of heated flow after it undergoes its initial expansion.

Since flow through an expansion fan is isentropic, p_t expansion is the same as p_{t2} . The static pressure after expansion of the heated flow is given by

$$\frac{p_{expansion}}{p_t \text{ expansion}} = \left[1 + \frac{(\gamma - 1) M_{expansion}^2}{2} \right]^{\frac{-\gamma}{\gamma-1}}, \quad (35)$$

where $M_{\text{expansion}}^2$ is the Mach number of the expanded flow after it has passed through the expansion fans once as determined by the Prandtl-Meyer expansion equations:

$$\nu(\theta) = \sqrt{\frac{\gamma+1}{\gamma-1}} \arctan\left(\sqrt{\frac{(\gamma-1)(M_i^2-1)}{\gamma+1}}\right) - \arctan(\sqrt{M_i^2-1}), \quad (36)$$

where θ is as defined above and is called the slip line, as the flows on either side have different Mach numbers but are parallel to each other and there is a discontinuity in density which is visible in Fig. 12. The equations above only apply near the end of the tube where a 2D approximation accurately captures the behavior of the flow. As you move closer to the centerline or further back, the expansion of the flow in the direction normal to the plane of analysis alters the flow and expansion fans start to interact with the expansion fans and slip lines across the center line. Once an expansion fan reaches the opposite slip line, Mach waves turn the heated flow into a more axial flow. The reduction in the slip line angle θ causes expansion fans of the flow downstream of the shock and outside of the slip line. When this expansion fan reaches the oblique shock, the Mach waves making up the new expansion fan turn the oblique shock towards the axial direction and weaken the shock as the downstream and upstream flows have a more similar Mach number and flow direction. This is visible in Fig. 14 as the c_p begins to even out in the shock and heated region.

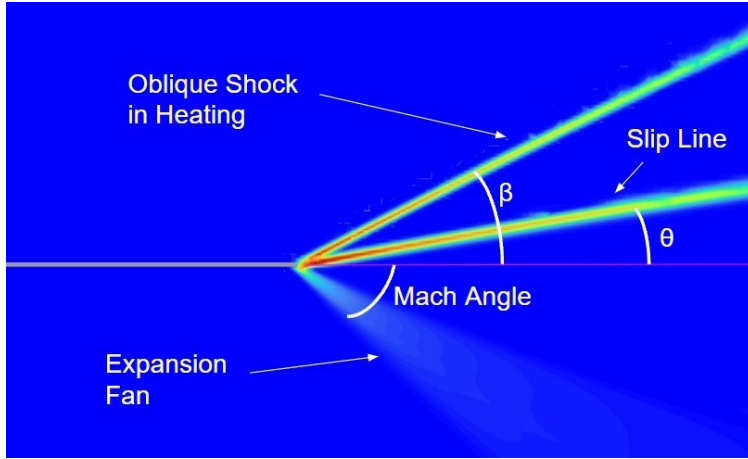


Fig. 12 Numerical Schlieren view of supersonic flow downstream of the duct exit. The three features are an oblique shock, a slip line and an expansion fan. The angles between these features and the axial vector are also labelled.

B. Numerical Calculation

1. Computational Setup

The CFD setup for supersonic calculations was slightly different from the subsonic setup. With regard to the geometry, the leading edge duct walls were also made to be of zero thickness such that the whole duct consisted of the infinitesimal wall (Fig. 13). This was done to best recreate the original case by Oswatitsch [1], in which supersonic flow

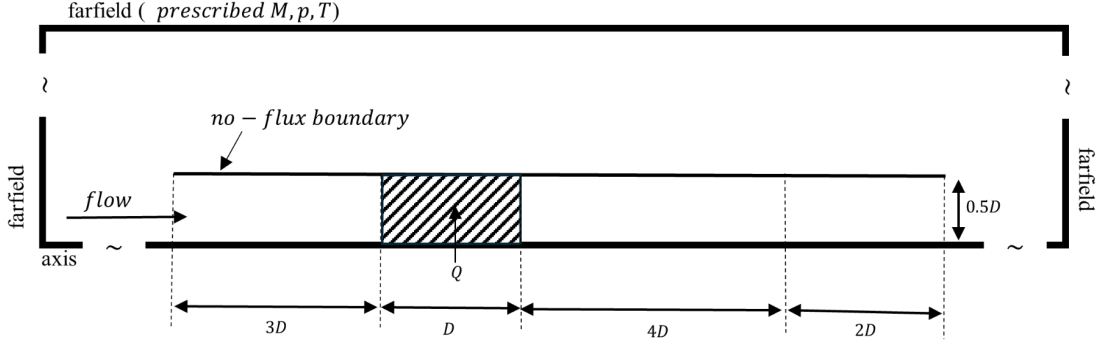


Fig. 13 Domain and duct geometry of supersonic CFD calculations.

does not see the thickness of the duct wall. The solver used third order schemes and the mesh was dynamically adapted based on Mach number and density gradients to ensure high quality convergence.

2. Thrust

For supersonic heating, there are two cases: Regime IV and Regime V. Numerical solutions have been obtained for Regimes V and IV. Preliminary numerical solutions for Regime IV will be presented later in Section X.

For Regime V, numerical calculations across a range of M_0 and T_{t2}/T_{t1} were all consistent with the zero thrust analytical solution.

3. Flow Topology

The streamlines for supersonic heating (Fig. 14) were as predicted from the analytical work. The flow enters the duct without any curvature and leaves with some expansion.

4. Shocks

For Regime V, beyond the normalised thrust, our numerical investigation extended to the quantitative flow features exiting the duct. Numerical results at $M_0 = 3.0$ agree strongly with analytical predictions (Fig. 15).

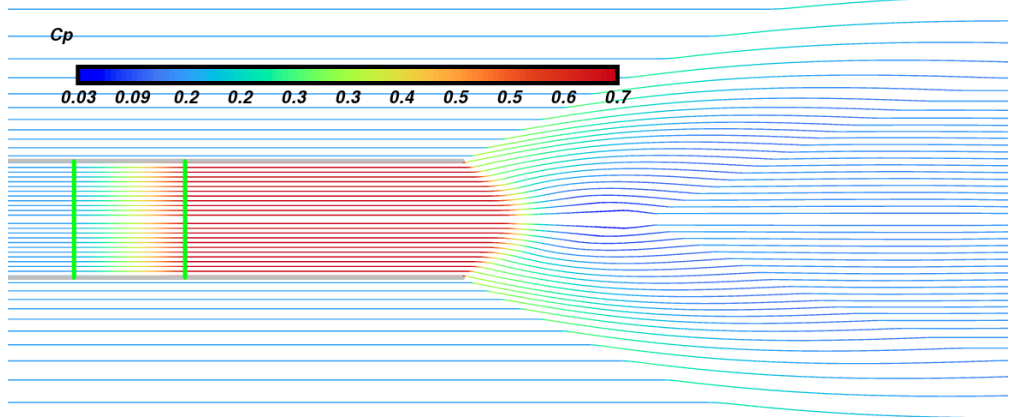


Fig. 14 Streamlines for supersonic heating at a freestream Mach number of 3.0. The streamline expansion is consistent with the analytical result.

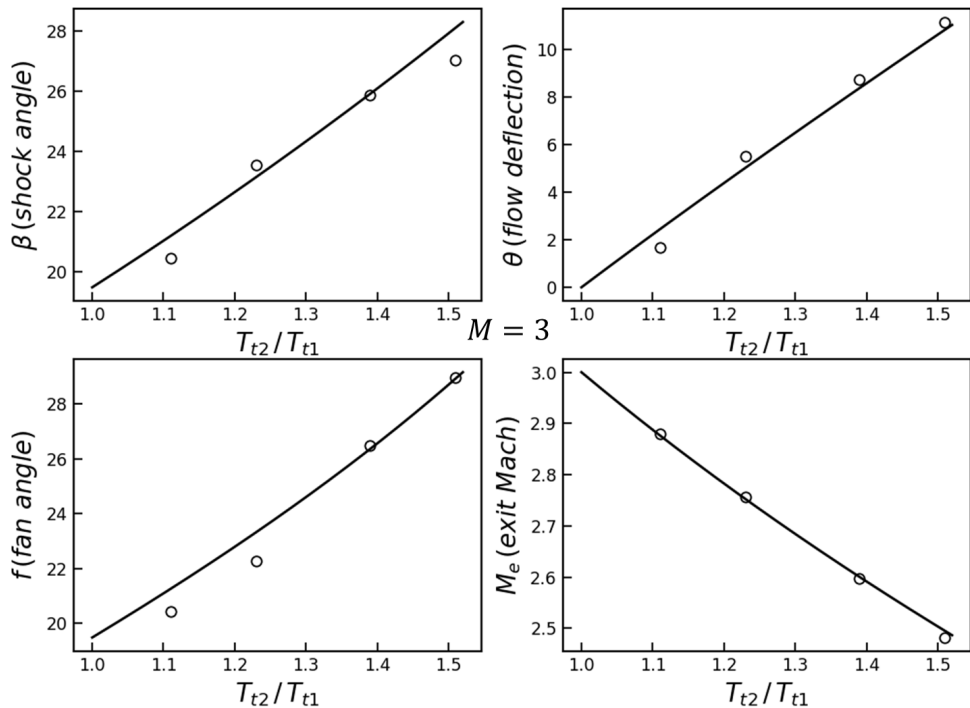


Fig. 15 Numerical results of shock angle, flow deflection, fan angle and exit Mach number compared to analytical curves at $M_0 = 3.0$ across a T_{t2}/T_{t1} from 1.1 to 1.5. Numerical results (circles) are consistent with the analytical curves.

VII. Quadrant IV: Supersonic Cooling

A. Analytical Calculation

The supersonic cooling regime is bounded from below by the limiting case in which the flow is cooled to $T_2 \rightarrow 0$, causing the exit Mach number to approach infinity ($M_2 \rightarrow \infty$). This lower bound can be expressed in terms of the exit

Mach number using the relation:

$$\tau_{\text{lim}} = \frac{(1 + \gamma M_0^2)^2 (\gamma + 1)}{2(\gamma M_0)^2 \left[1 + \left(\frac{\gamma - 1}{2} \right) M_0^2 \right]} \quad (37)$$

It is worth noting that the critical temperature ratio τ_{cr} (Eq.37), which defines the upper boundary of Regime V, and the limiting temperature ratio τ_{lim} , which defines the lower boundary, exhibit the same trend. This is because they are related by the expression

$$\tau_{\text{cr}} = \frac{\gamma^2}{(\gamma + 1)(\gamma - 1)} \cdot \tau_{\text{lim}}. \quad (38)$$

1. Thrust

Similar to the case of slight heating in supersonic flow, in Regime V, on the cooling side, the flow remains supersonic throughout the duct. The flow is unchanged from station 0 to station 1. Flow properties at station 2 are calculated using Eqs. 24-28, and in this regime, the flow exits the duct at a supersonic underpressure relative to ambient. Like the heating case in Regime V, a control volume analysis on CV_{ext} , as expected, reveals that net thrust is zero. The zero-thrust result is also consistent with the flow pattern, as neither the supersonic inlet or exit flow can produce thrust on an infinitesimally thin duct wall.

2. Shocks

The cooling case is highly analogous to the heating case, but with geometric features reflected across the wall of the ramjet. The pressure inside the stovepipe ramjet drops according to Eq. 4 from the freestream to the post-cooling pressure. This lower pressure will cause streamlines to converge once the flow exits the tube and forces the supersonic freestream to expand into the area around the ramjet to prevent a pressure discontinuity. The equilibrium between the adjustment of the freestream and the expansion of the cooled flow occurs when $p_{\text{expansion}} = p_{\text{shock}}$, where $p_{\text{expansion}}$ is the static pressure after the expansion of the freestream flow and p_{shock} is the static pressure downstream of the oblique shock in the cooled flow. The pressure ratio across an oblique shock is given by Eqs. 33-36, where M_2 replaces M_0 . Similar limitations hold for how far these equations can be applied from the edge of the ramjet as for the heating case. Fig. 24 shows strong agreement between the analytical model and the numerical model.

B. Numerical Calculation

1. Thrust

For supersonic cooling, the only possible solution is Regime V. Similar to Regime V of the supersonic heating case, numerical calculations with varying M_0 and T_{t2}/T_{t1} all agreed with the zero thrust result of the analytical work.

2. Flow Topology

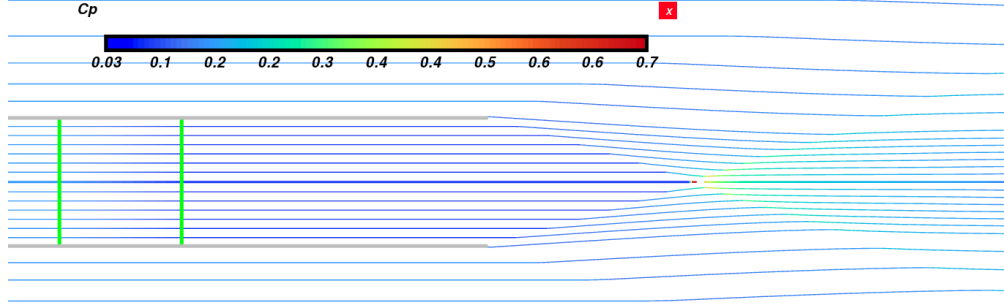


Fig. 16 Streamlines for supersonic cooling at a freestream Mach number of 3.0. The streamline contraction is consistent with the analytical result.

Streamlines for supersonic cooling obtained from numerical calculation (Fig. 16) were consistent with analytical results. Contrary to the supersonic heating case, the flow enters the duct with zero curvature and leaves with some contraction.

3. Shocks

Whilst numerical validation of the shock geometries for supersonic cooling could not be performed for a wide range of M_0 and T_{t2}/T_{t1} as in Section VI.B.4, several independent numerical data points agreed with analytical results. There is high confidence that this is true across all M_0 and T_{t2}/T_{t1} ranges of the supersonic cooling case.

VIII. Miscellaneous Topics

A. Entropy Generation and its Relationship to Drag

The analytical and numerical work in this report show that in Regime V of supersonic heating and cooling, the thrust is zero (rather than some finite positive or negative value). This may initially seem contradictory to Oswatitsch's Theorem [5], which relates the integral of entropy flow to the drag of a body. In other words, the lack of drag despite the entropy generation (or rejection) at the heat exchange region in the duct may conflict with Oswatitsch's findings.

However, it is important to note that Oswatitsch's Theorem [5] is founded upon the assumption of zero heat exchange between the body and the flowing gas. As such, the theorem does not apply to this problem.

In fact, Kuchemann [6] identifies an earlier 1959 work by Oswatitsch [1] that addresses the particular paradox of entropy generation in a supersonic stovepipe ramjet. The explanation is that, unlike the subsonic cases, the heat exchanger contributes not only to heat generation but also to shock generation in the external stream, as we have verified analytically and numerically. These two effects entirely cancel each other out, resulting in zero drag. The entropy variation across the domain $\Delta s = C_p \ln \left(\frac{T_t}{T_{t0}} \right) - R \ln \left(\frac{p_t}{p_{t0}} \right)$ is presented in Figs. 17 and 18, where two regions of entropy

generation, the heating region and the shock region, can be seen.

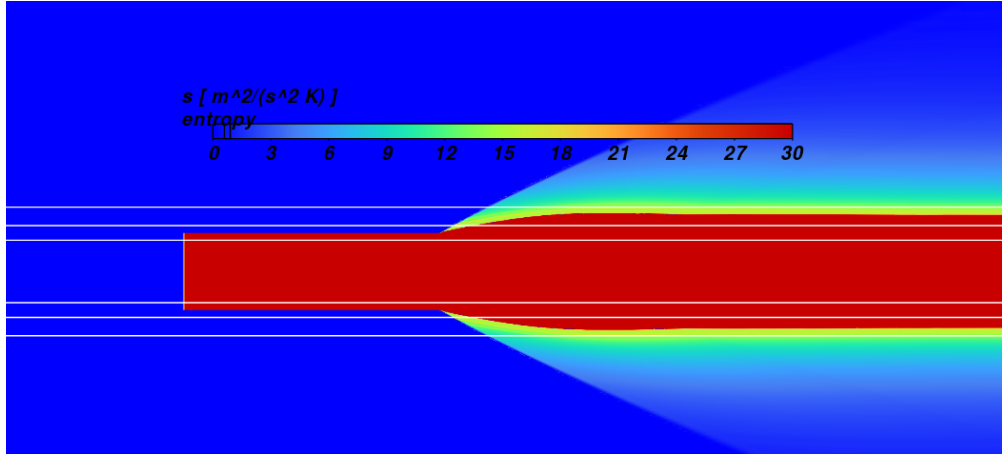


Fig. 17 Entropy change for supersonic heating at a freestream Mach number of 3 and the line probe locations for Fig. 18.

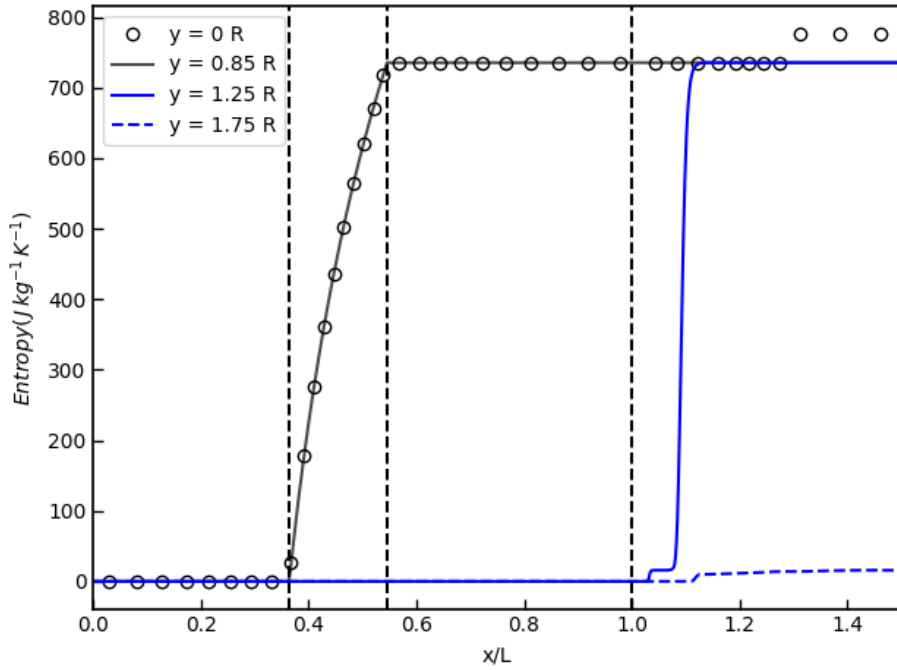


Fig. 18 Entropy variation at different radial locations along the axis (L-duct length), at a freestream Mach number of 3.0. The vertical lines denote the start and end of the heating region and the end of the ramjet, respectively.

B. Practical Application of Supersonic Cooling

Cooling of the air going into jet engines has been tested and demonstrated to increase the specific thrust of engines by increasing the maximum possible mass flow [7]. This is achieved by using cryogenic fuel passed in fins upstream

of the compressor. Such a design increases the T_{t_4}/T_{t_2} that can be achieved for a fixed T_{t_4} value, which is fixed by technology limits and increases efficiency as less air needs to be bled to maintain the turbine temperature below the service temperature. Accordingly, a proper understanding of the impact of choking the nozzle, which maximizes the specific thrust of the engine, motivates further study on the relationship between cooling fin geometry and drag impacts.

IX. Conclusion

This report began by laying out the prior work by Oswatitsch on subsonic and supersonic heating of a stovepipe ramjet [1]. Through analytical and numerical studies, it was found that Oswatitsch work was correct but incomprehensive, limited only to Regime I and Regime V (heating) of Fig. 6. In this report, the stovepipe ramjet problem was extended to Regimes II, III, IV and V (cooling), described comprehensively with analytic solutions. Furthermore, all but Regime IV were validated numerically. Succinctly, this entire project boils down to Figs. 5 and 6, together called "Four Quadrants, Five Regimes."

X. Future Work

To complete the full picture of this problem, it is desirable to conduct a full numerical validation of Regime IV. Whilst the timeline proved to be a constraint, the team has obtained preliminary numerical results for the regime. Figs. 25-29 in the Appendix visualise these results as plots of Mach number contour, Schlieren image, total temperature contour and streamlines. The bow shocks are resolved well, however, the flow seems to choke downstream of the heat addition region of the duct. Since this was not captured in the analytical solution, it must be investigated whether or not such regimes do in fact exist. Furthermore, more numerical work must be done in an attempt to obtain solutions to cases where the flow in the duct does not choke.

References

- [1] Oswatitsch, K., *Gas Dynamics*, Applied mathematics and mechanics, Academic Press, 1956. URL <https://books.google.com/books?id=mfZQAAAAMAAJ>.
- [2] Shapiro, A. H., and Sonin, A. A., *Advanced Fluid Mechanics Problems*, 1986.
- [3] Greitzer, E. M., Tan, C. S., and Graf, M. B., *Internal Flow: Concepts and Applications*, 1st ed., Cambridge University Press, 2004. <https://doi.org/10.1017/CBO9780511616709>, URL <https://www.cambridge.org/core/product/identifier/9780511616709/type/book>.
- [4] Shapiro, A., *The Dynamics and Thermodynamics of Compressible Fluid Flow, Volume 1*, Engineering special collection, Wiley, 1953. URL <https://books.google.com/books?id=lPMmAAAAMAAJ>.
- [5] Oswatitsch, K., “The Drag as Integral of the Entropy Flow,” *Contributions to the Development of Gasdynamics: Selected Papers, Translated on the Occasion of K. Oswatitsch’s 70th Birthday*, edited by K. Oswatitsch, W. Schneider, and M. Platzer, Vieweg+Teubner Verlag, Wiesbaden, 1980, pp. 2–5. https://doi.org/10.1007/978-3-322-91082-0_1, URL https://doi.org/10.1007/978-3-322-91082-0_1.
- [6] Kuchemann, D., *The Aerodynamic Design of Aircraft*, Amer Inst of Aeronautics &, Reston, Va, 2012.
- [7] Sloop, J. L., “Liquid hydrogen as a propulsion fuel, 1945-1959,” , Jan. 1978. URL <https://ntrs.nasa.gov/citations/19790008823>, nTRS Author Affiliations: National Aeronautics and Space Administration NTRS Report/Patent Number: NASA-SP-4404 NTRS Document ID: 19790008823 NTRS Research Center: Headquarters (HQ).

Appendix

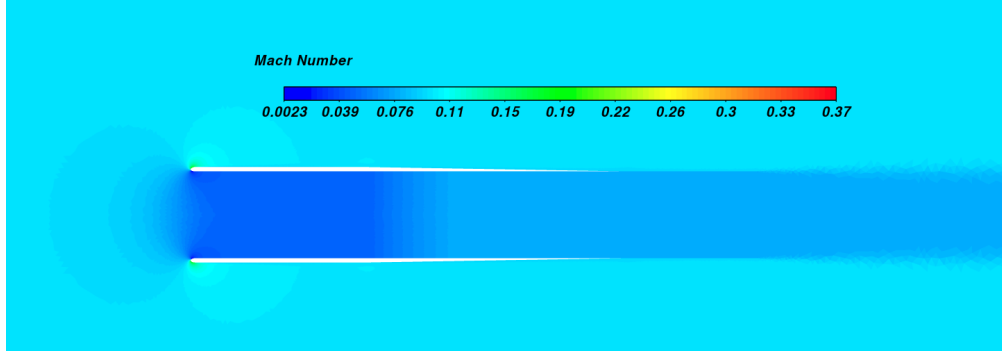


Fig. 19 Mach contour for subsonic heating at $M_0 = 0.1$.

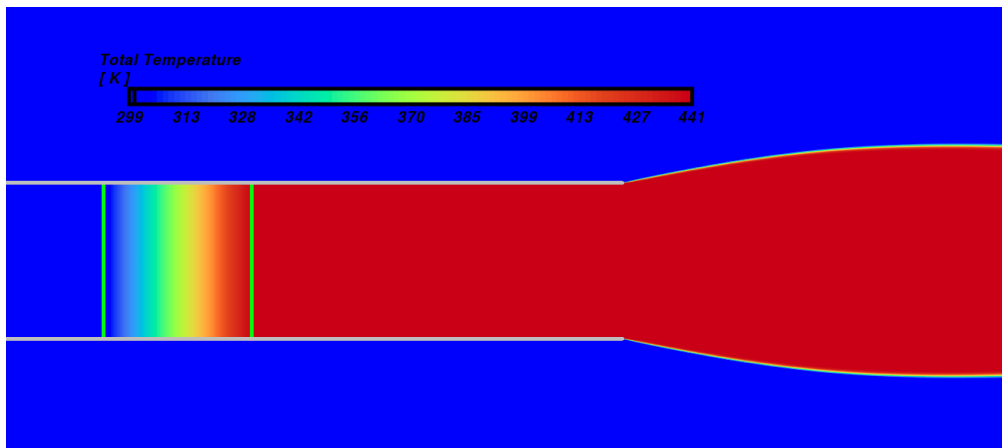


Fig. 20 Total temperature contour for supersonic heating at $M_0 = 3.0$. The contour clearly shows the heat addition process and the increased total temperature downstream of the region.

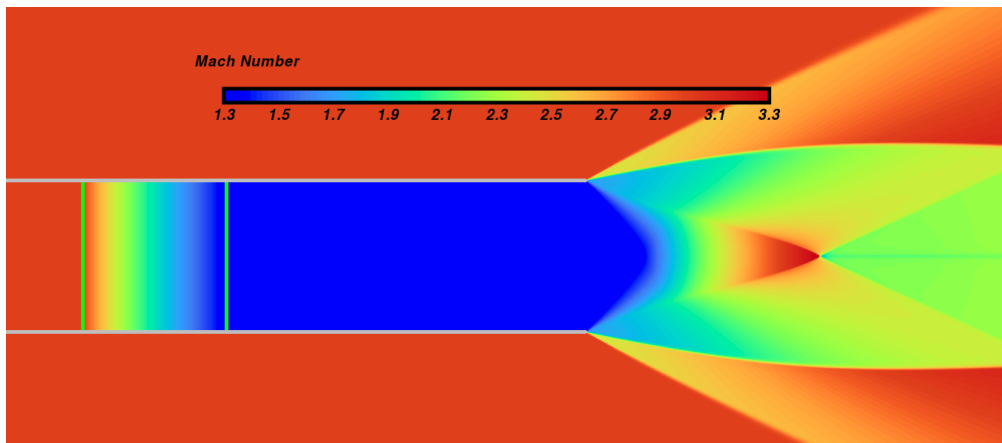


Fig. 21 Mach contour for supersonic heating at a freestream Mach number of 3.0. The expansion fan, slip line and oblique shock are consistent with the analytical result.

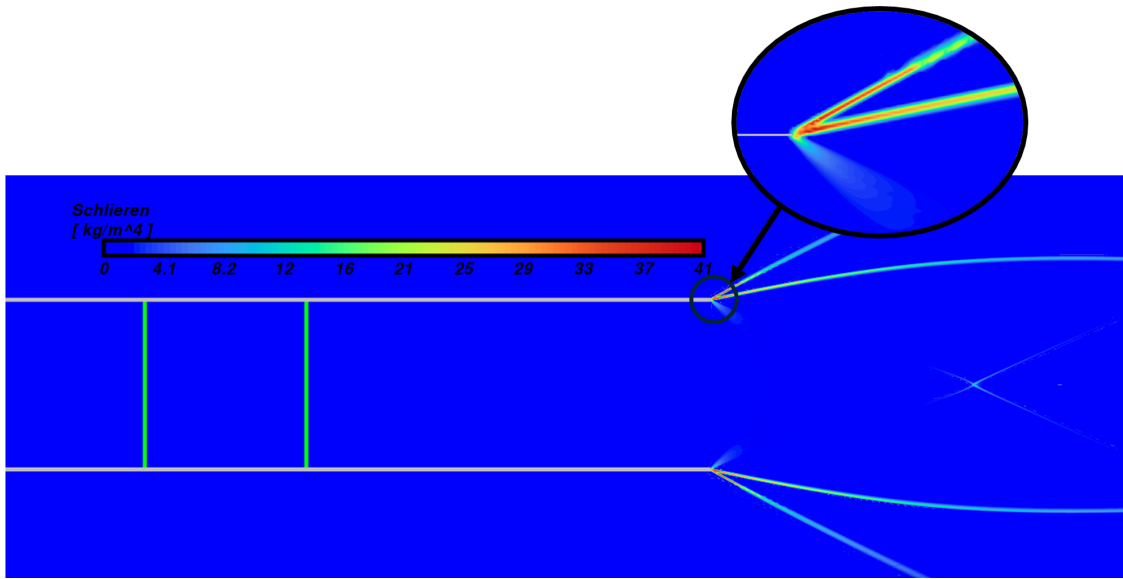


Fig. 22 Numerical Schlieren plot for supersonic heating at a freestream Mach number of 3.0. The expansion fan, slip line and oblique shock are consistent with the analytical result.

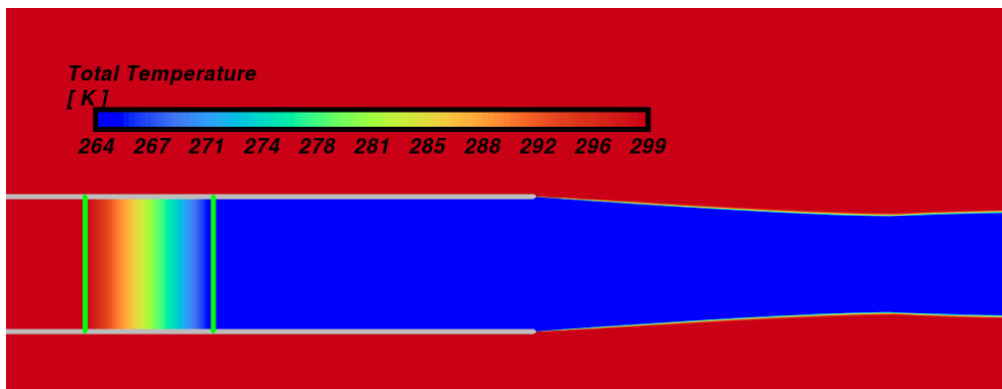


Fig. 23 Total temperature contour for supersonic cooling at $M_0 = 3.0$. The contour clearly shows the heat rejection process and the decreased total temperature downstream of the region.

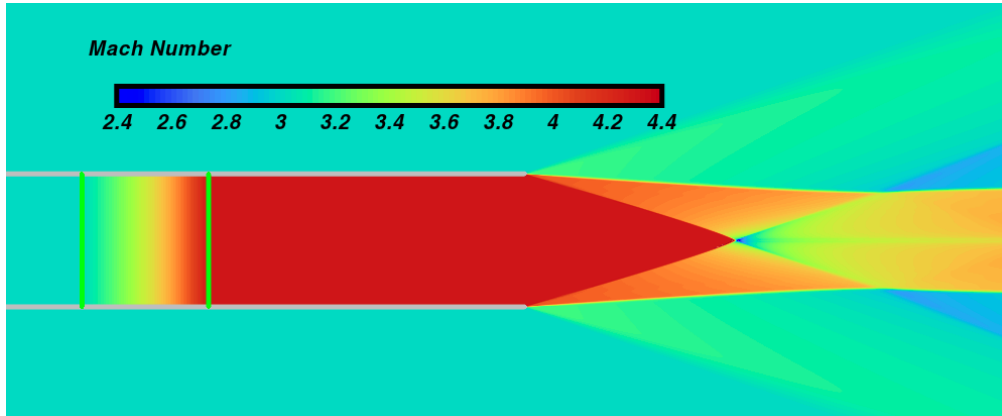


Fig. 24 Mach contour for supersonic cooling at a freestream Mach number of 3.0. The expansion fan, slip line and oblique shock are consistent with the analytical result. The geometry is identical to the supersonic heat addition case but inverted about the duct wall.

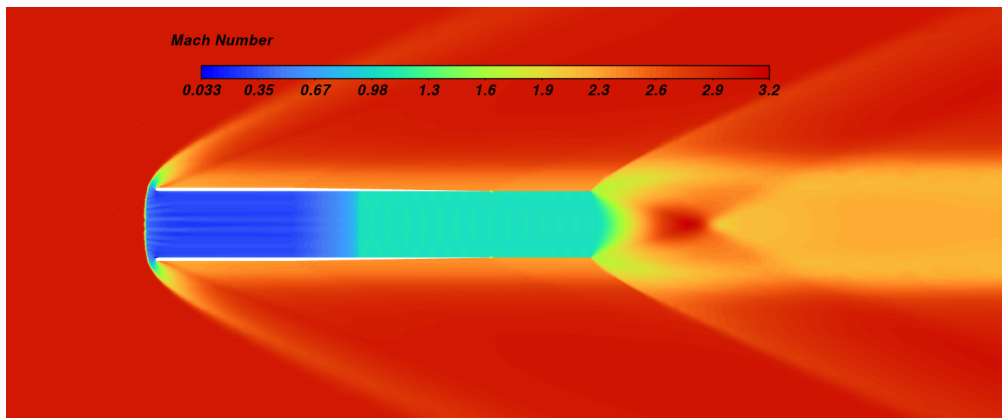


Fig. 25 Preliminary numerical Mach contour of Regime IV at $M_0 = 3.0$. There is a clean bow shock just upstream of the duct inlet.

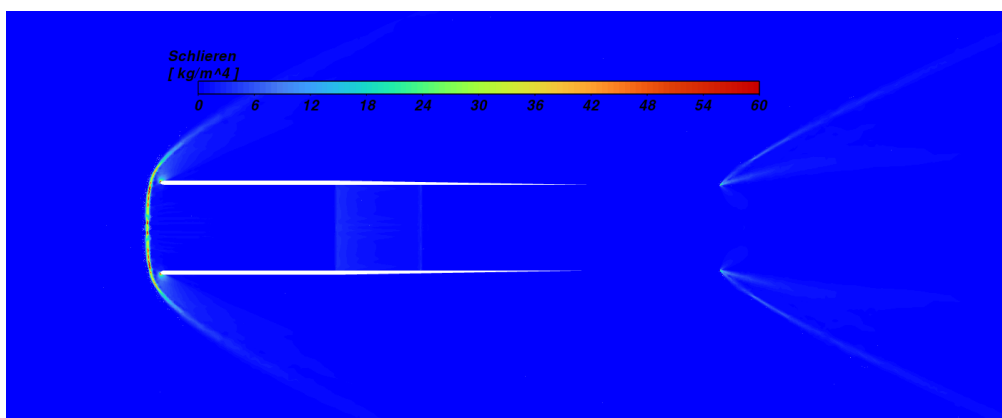


Fig. 26 Preliminary numerical Schlieren plot of Regime IV at $M_0 = 3.0$. The bow shock is clearly visible, as well as vague signs of shock-like features downstream of the duct exit.

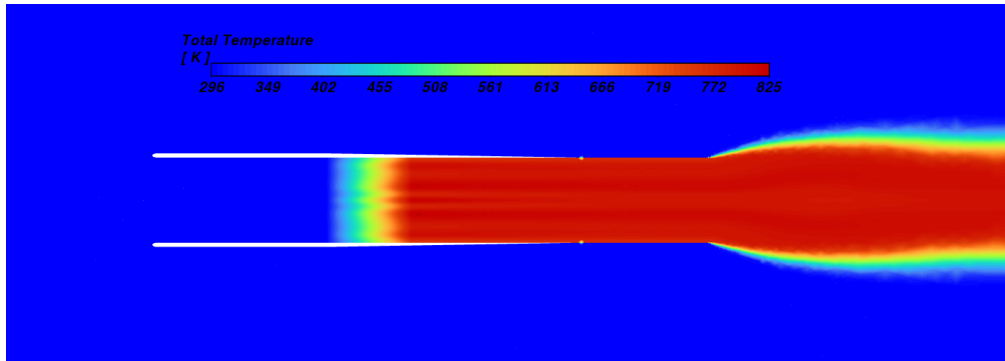


Fig. 27 Preliminary numerical total temperature contour of Regime IV at $M_0 = 3.0$. There is no change in total temperature until the heat addition region, downstream of which there is a largely uniform increased total temperature.

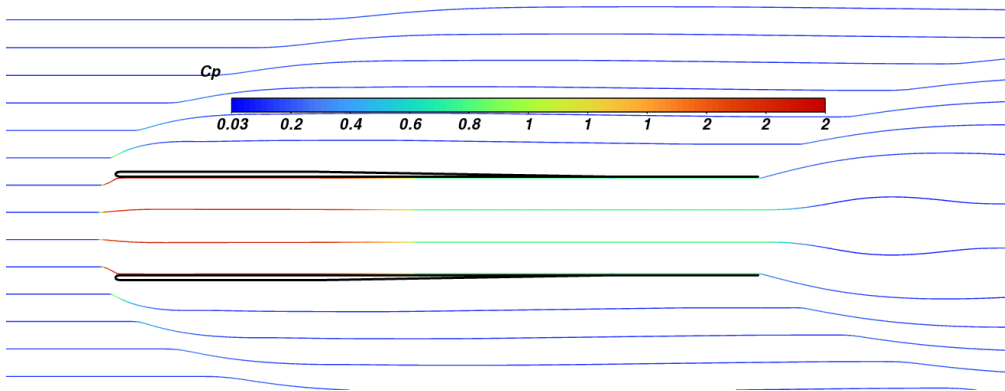


Fig. 28 Preliminary numerical streamlines of Regime IV at $M_0 = 3.0$. A bow shock just upstream of the duct inlet and flow expansion downstream of the duct exit are depicted.

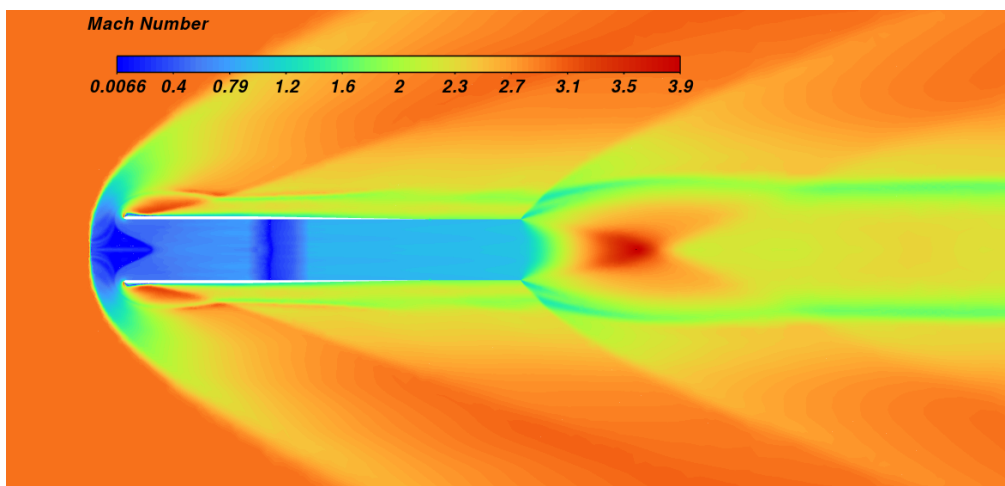


Fig. 29 A second preliminary numerical Mach contour of Regime IV at $M_0 = 3.0$. There is a clean bow shock just upstream of the duct inlet.